Japanese Journal of Applied Physics

The Japan Society of Applied Physics

PROGRESS REVIEW

Spontaneous orientation polarization in organic light-emitting diodes

Japanese Journal of Applied Physics **58**, SF0801 (2019) **PROGRESS REVIEW**
https://doi.org/**10.7567/1347-4065/ab0de8**

Spontaneous orientation polarization in organic light-emitting diodes

Yutaka Noguchi[1*], Wolfgang Brütting[2], and Hisao Ishii[3]

[1]*School of Science and Technology, Meiji University, Kanagawa 214-8571, Japan*
[2]*Institute of Physics, University of Augsburg, 86135 Augsburg, Germany*
[3]*Center for Frontier Science, Chiba University, Chiba 263-8522, Japan*

[*]E-mail: noguchi@meiji.ac.jp

Received November 29, 2018; accepted February 22, 2019; published online May 24, 2019

Spontaneous orientation polarization (SOP) is inherent in the evaporated films of many organic semiconducting molecules with a permanent dipole moment. A significant electric field is formed in the film due to SOP. Consequently, the properties of organic light-emitting diodes (OLEDs) incorporating such films are influenced. The polarization charge appearing at heterointerfaces dominates the charge injection and accumulation properties. Moreover, SOP correlates with device degradation. In this article, we review the SOP of organic semiconductor films and its influences on the device properties of OLEDs. © 2019 The Japan Society of Applied Physics

1. Introduction

Because of their anisotropic molecular shape, the majority of organic semiconductors exhibit orientational degrees of freedom. The microscopic orientation of molecules in thin films has a strong impact on macroscopic properties such as charge carrier transport and optical properties as well as on the efficiency of organic light-emitting diodes (OLEDs). Initially, organic semiconductor films used in OLEDs were typically considered amorphous, where the molecules are "randomly oriented" and thus the macroscopic properties are isotropic. However, the amorphous state may have short-range order, even though it has no long-range order. Many spectroscopic studies have evaluated molecular orientation in non-crystalline organic semiconductor films since 1980s.[1)] In 2009, Refs. 2, 3 revisited the molecular orientation in the amorphous organic semiconductor films, and clearly demonstrated their impact on the device performances of OLEDs. Today, molecular orientation has been recognized as key parameter in modern OLEDs, e.g., the in-plane orientation of the emitter's transition dipole moment (TDM) enhances the light outcoupling efficiency, and π-stacking along the out-of-plane direction improves the electrical conductivity.[2–9)] Furthermore, the asymmetric structure of the molecule induces a permanent dipole moment (PDM), and the average orientation of PDMs to a certain direction leads to macroscopic orientation polarization in the film.[10)] Since orientation polarization induces polarization charges at heterointerfaces accompanied by an electric field in the film, one has to consider the device properties taking into account these factors in addition to molecular orientation itself.[11–20)]

In 1972, Ref. 21 reported spontaneous build-up of surface potential up to 100 V at 100 μm for a multilayer of eight gases (^{12}CO, ^{13}CO, NO, N_2O, SO_2, NH_3, H_2O, and acetone) physisorbed on a cold surface below 100 K. The surface potential originates from spontaneous ordering of PDMs, i.e., spontaneous orientation polarization (SOP). Since then, the SOP of condensates of water ice, alcohols, ketones, ethers, and other materials have been widely investigated.[22–30)] The PDM of these molecules are typically less than 0.5 D, and the electric field formed due to SOP is in the range of 1–120 mV nm^{-1} at around 40 K. The negative electric field, corresponding to the negative end of PDM toward the vacuum side, has been observed in addition to the positive electric field, e.g., H_2O (1.85 D): -36 mV nm^{-1} at 30 K,[29)] CF_3Cl (0.5 D): -42.5 mV nm^{-1} at 40 K,[27)] and N_2O (0.167 D): 97 mV nm^{-1} at 40 K.[26)] The SOP decays for films deposited at higher temperatures and typically disappears around 80 K.

Surprisingly, in the case of organic semiconductors, SOP occurs at room temperature. The first direct observation of SOP in organic semiconductors was reported by Ref. 10 in 2002. They observed the surface potential of an Alq_3 film, which linearly grows with increasing film thickness. The surface potential reaches 28 V at 560 nm, and thus a so-called giant surface potential (GSP) is formed; however, GSP diminishes via the light absorption of the Alq_3 film. Complementary studies using optical second harmonic generation revealed that GSP originates from SOP, i.e., the spontaneous order of the PDMs of Alq_3.[10,31)] At the initial stage, researchers have focused on the photo-induced decay mechanism of GSP mainly motivated by interest in fundamental material science rather than device physics.[10,32–35)]

GSP/SOP is not a unique property of Alq_3. Refs. 16, 39 revealed that GSP is quite common in the evaporated films of OLED materials, including thermally activated delayed fluorescence (TADF) emitters,[36–38)] and various kinds of emitters and electron transporters. However, the mechanism of the spontaneous formation of orientation polarization is still not completely understood. Reference 40 proposed the "asymmetric dice model" in which the driving force of the molecular orientation is attributed to the biased distribution of the stable posture of molecules on the film surface due to asymmetric molecular shape. Their model qualitatively explained the GSP characteristics of Alq_3 and its derivative ($Al(7\text{-}Prq)_3$) films. Recently, Ref. 41 have succeeded in mimicking the GSP of several materials using atomistic simulations. They pointed out that short-range van der Waals interactions between the molecule and the surface during deposition dominate the driving force of the anisotropic molecular orientation, while intermolecular dipole–dipole interactions suppress the orientation degree. The contribution of the PDM interaction to the SOP formation is also supported by experimental results. Refs. 42, 43 reported SOP in the guest–host systems consisting of polar and nonpolar molecules. The degree of PDM orientation is enhanced by diluting the polar molecules in a nonpolar host,

which indicates that the PDM interaction acts as a negative factor in SOP formation.

Because of the photoinduced decay nature,[10,31–33] GSP has initially was not considered as an important parameter in terms of device properties. It was believed that no influences remain in actual OLED devices after vanishing GSP due to the absorption of the ambient light and emission from the device itself. However, interestingly, Ref. 11 reported the influence of SOP on the charge injection and accumulation characteristics of an Alq_3-based OLED in 2000, that is two years earlier than the first GSP report. They concluded on the presence of "fixed negative interfacial charge" between Alq_3 and α-NPD layers by using impedance spectroscopy. Eight years later, Refs. 13, 16 pointed out that the interface charge and GSP have a common origin, namely the polarization charge due to SOP in the evaporated film. SOP is maintained in actual devices and thus induces fixed charges at the heterojunctions in the devices. Their results also suggest an alternative mechanism of GSP decay which was under debate at that time;[10,32–35] the molecular order does not vanish due to light absorption, but GSP decays due to the photogenerated carriers in the film.

The negative polarization charge due to SOP at the α-NPD/Alq_3 interface causes hole injection at voltages even lower than the built-in voltage of the device.[11,12] The injected holes are accumulated at the interface to compensate for the negative interface charge during device operation. Importantly, the accumulated charge is the real charge although the interface charge is the polarization charge, and the amount is comparable to the maximum amount of the accumulated charge in operating OLEDs.[16,44–47] The presence of the accumulated charge near the emission zone can enhance the recombination probability, but the charged species can also act as an exciton quencher.[48–52] Moreover, the concentration of the emission zone leads to faster degradation.[50,53] On the other hand, the positive polarization charge at the Alq_3/cathode interface is suggested to assist the electron injection through formation of the electric double layer or gap states at the interface.[18,54,55]

Polar films are included in common organic thin film devices, since PDM is inherent to many organic semiconductors. SOP has not been considered as a significant factor in device performance, though it may be used unintentionally. In terms of device optimization, SOP should be taken into account as well as other common material properties, such as energy levels and charge carrier mobility. In this review, we describe the current understanding of SOP and its influences on device properties.

2. Spontaneous orientation polarization in organic films

2.1. Basics of SOP and GSP

We consider a thin film composed of polar molecules where the film has a spontaneous polarization $\mathbf{P}_0$ (Fig. 1). $\mathbf{P}_0$ is defined as the net PDM per unit volume; i.e., $\mathbf{P}_0 = \sum_i \mathbf{p}_i / L^3$, where $\mathbf{p}_i$ is the PDM of ith molecule and L^3 is the volume of the film. If the film consists of a single component, the contribution of each molecule along the surface normal (unit vector: $\hat{\mathbf{z}}$) is given by

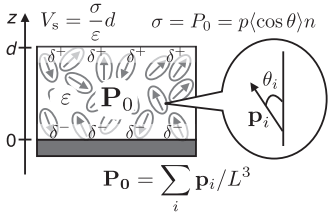

Figure 1. Schematic illustration of the organic thin film with spontaneous orientation polarization. L^3 is the volume of the film.

$$\mathbf{p}_i \cdot \hat{\mathbf{z}} = p \cos\theta_i, \tag{1}$$

and thus,

$$P_0 = \mathbf{P}_0 \cdot \hat{\mathbf{z}} = \frac{p \sum_i \cos\theta_i}{L^3} = p \langle \cos\theta \rangle n, \tag{2}$$

where n is the density of the molecule, and $\langle \cos\theta \rangle$ is the average orientation degree of PDM with respect to the surface normal direction, namely,

$$\langle \cos\theta \rangle = \frac{\sum_i \cos\theta_i}{nL^3}. \tag{3}$$

Note that $\sigma = P_0$ corresponds to the polarization charge density induced on the film surface. If we assume a certain distribution function, the average orientation degree can also be described as[43]

$$\langle \cos\theta \rangle = \frac{\sum_k \Phi(\theta_k) \cos\theta_k}{nL^3}. \tag{4}$$

Here, $\Phi(\theta_k)$ indicates the number of molecule whose PDM is pointing at a particular orientation angle, θ_k, in the volume. Because of the nonlinear (cosine) contribution of the PDM orientation angle to SOP, the most preferential orientation angle of PDM, θ_m, does not generally correspond to the average orientation degree. Therefore, Eq. (4) is useful to investigate the relations between SOP and molecular orientation.[43]

The spontaneous polarization forms the electric field ($\mathbf{P}_0/\varepsilon$) in the film, where ε is the dielectric constant. If $\mathbf{P}_0$ is uniform throughout the film, the potential at the film surface with reference to the substrate, V_s, is given by

$$V_s = \int_0^d \mathbf{P}_0/\varepsilon \cdot d\mathbf{z} = \frac{p\langle\cos\theta\rangle n}{\varepsilon} d = \frac{\sigma}{\varepsilon} d, \tag{5}$$

where d is film thickness. The surface potential is proportional to the film thickness if P_0 is constant. This property appears in GSP, and thus the Kelvin probe method is often used to examine SOP characteristics.

2.2. Materials exhibiting SOP and their characteristics

In Fig. 2, we summarize the molecules that exhibit SOP in the evaporated film.[10,18,39,40,56,57] Calculated PDM intensities and GSP slopes reported in previous studies are also shown. The molecules are mostly electron transport or light emitting materials, including TADF[36–38] and Ir-based phosphorescent emitters, which are commonly used in OLEDs. In the research field of OLEDs, molecular orientation is often evaluated in terms of TDM orientation;[3,9] therefore the materials are divided into three groups with different qualitative TDM orientations: random, unknown, and horizontal.

Figure 3 shows the surface potential of the evaporated films of several materials. GSP behavior, i.e., linear growth

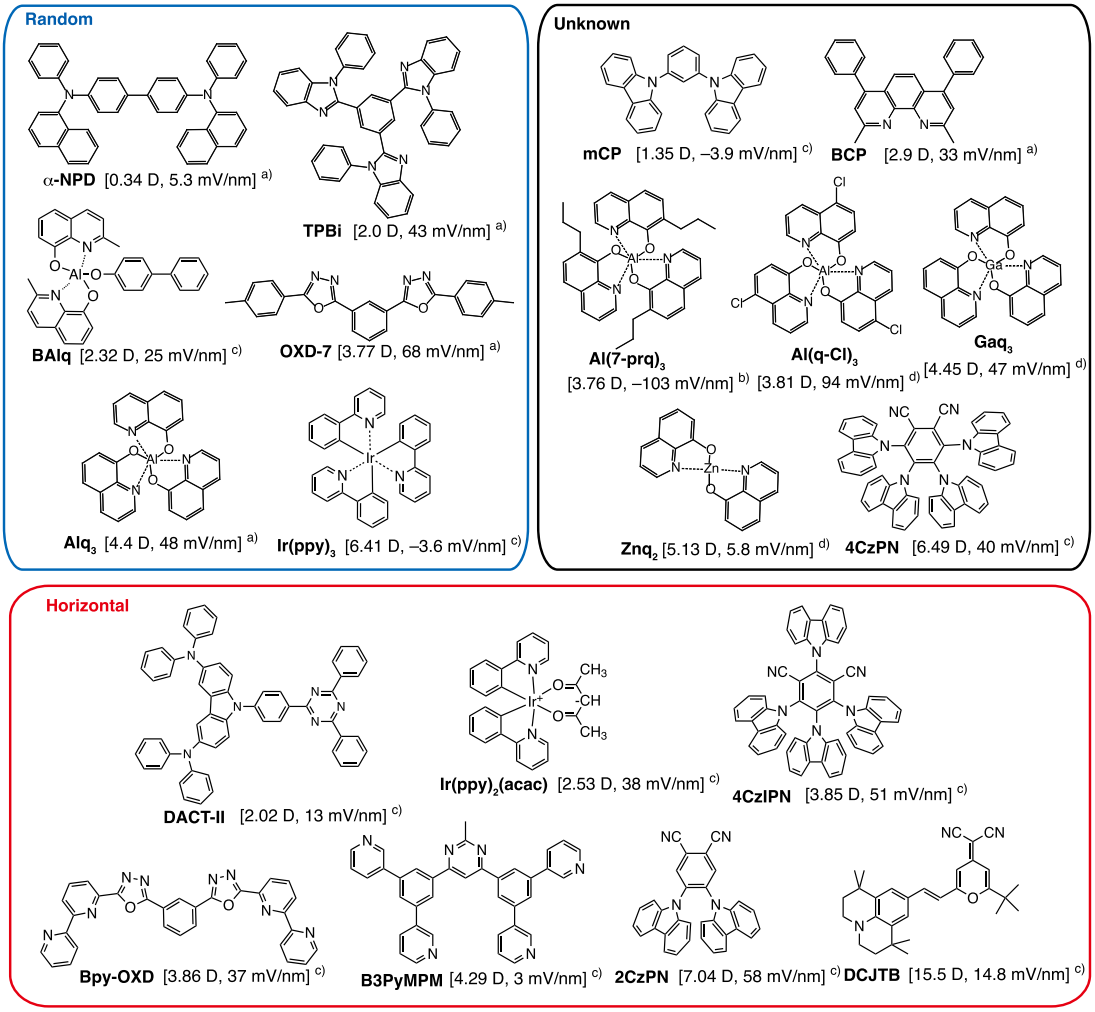

Figure 2. (Color online) Molecular structures of the organic materials exhibiting SOP in the evaporated film. The PDM of each molecule was calculated using Gaussian16 (DFT/B3LYP with an LANL2DZ basis set for $Ir(ppy)_3$ and $Ir(ppy)_2(acac)$, and a 6-31G* basis set for all other molecules). The reported GSP slope is indicated in brackets, where the data indicated by a), b), c), and d) are taken from Refs.16, 18, 39 and 56, respectively (see also Fig. 5). The molecules were divided into three classes (random, unknown, and horizontal) based on their reported TDM orientations.[2,38,58–62] Note that α-NPD, $Ir(ppy)_3$, mCP, and B3PyMPM show only weak surface potential. The correct terminology of the molecule "α-NPD" presented in this figure is "NPB", though both terms have been commonly used for this molecule. Adapted with permission from Ref. 39.

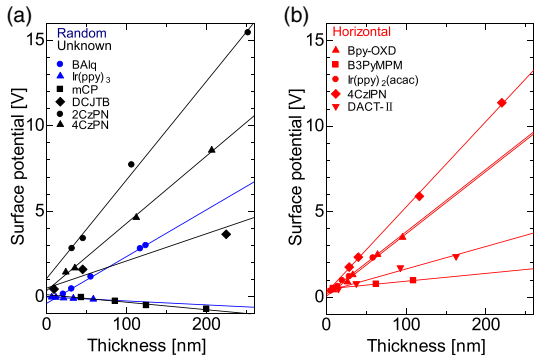

Figure 3. (Color online) Surface potentials of evaporated organic films as a function of film thickness. (a) "Random" and "Unknown" materials. (b) "Horizontal" materials. Reprinted with permission from Ref. 39.

of the surface potential as a function of the film thickness, is observed, indicating that SOP is inherent in these films. Some of them exhibit surface potential exceeding several volts at film thicknesses over ∼100 nm. Such behavior corresponds to typical GSP characteristics. On the other hand, $Ir(ppy)_3$, mCP, and B3PyMPM films exhibit only weak surface potential. As evident in the results, the GSP/SOP is very common in films with randomly oriented TDMs as well as in films with the horizontally oriented TDMs.

SOP appears in the films regardless of TDM orientation type. TDM orientation is typically evaluated by optical measurements, where the head and tail of the molecule are indistinguishable because these methods evaluate the orientation of TDM intensity ($\propto\langle\cos^2\theta_t\rangle$, where θ_t indicates the orientation angle of TDM). Moreover, random TDM orientation does not necessarily indicate the random orientation of the symmetry axis of the molecule. For example, Ref. 63 reported that the molecular orientation in the $Ir(ppy)_3$ film has random TDM orientation. On the other hand, SOP originates from the PDM orientation, including its head-to-tail direction, as it is proportional to $\langle\cos\theta\rangle$. SOP is therefore inherent even in films with "randomly oriented" TDMs.

Of course, TDM and PDM orientations are not independent, as both of them are related to the orientation of the molecular frame. Therefore, the combined analysis of TDM and PDM orientations can be used for accurate estimation of molecular orientation. Reference 43 proposed a method to determine the distribution range of the preferable molecular

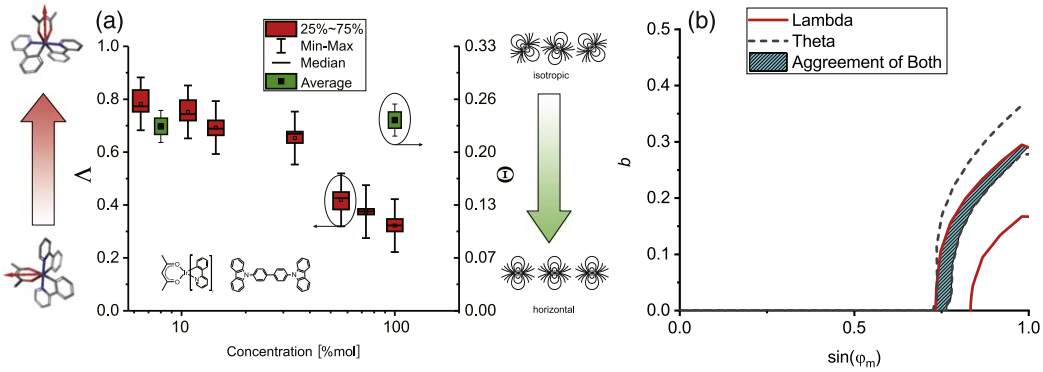

Figure 4. (Color online) (a) Experimentally determined orientation degrees of PDM (Λ) and TDM (Θ) of the guest–host system, where $Ir(ppy)_2(acac)$ and CBP are used as the guest and host, respectively. Λ corresponds to $\langle \cos\theta \rangle$, while Θ corresponds to $\langle \cos^2\theta_t \rangle$ in the main text. (b) The possible orientations of molecular symmetry axes of $Ir(ppy)_2(acac)$ estimated from the combined analysis of PDM and TDM orientations. The Gaussian distribution of the molecular orientation angle is assumed, where the peak angle is φ_m with a standard deviation of b. Note that the orientation angle is defined with reference to the in-plain axis. Adapted with permission from Ref. 43. Copyright 2018 American Chemical Society.

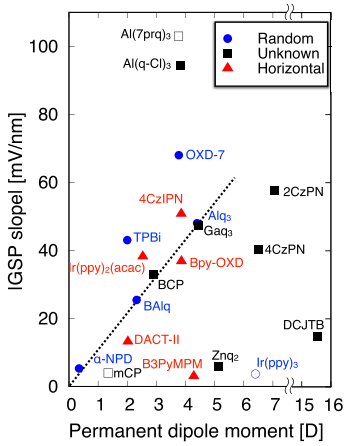

Figure 5. (Color online) Relationship between the absolute value of the GSP slope and PDM intensity for various organic materials. Each symbol indicates the TDM orientation in evaporated films with random (blue circles), unknown (black squares), and horizontal (red triangle) molecular orientations. Open symbols indicate negative GSP. Note that the GSP slope for DCJTB was variable, probably depending on the details of the film formation conditions. The GSP slope for DCJTB was observed from 7 to 25 mV nm^{-1}, and the average was 14.8 mV nm^{-1}. For TPBi, a larger GSP is also reported (~70 mV nm^{-1})[41]. Reprinted with permission from Ref. 39.

orientation angle based on the observation of TDM and PDM orientations (Fig. 4). They estimate the molecular orientation of typical phosphorescent emitters, $Ir(ppy)_3$ and $Ir(ppy)_2(acac)$, in a guest–host system, where the nonpolar molecule, CBP or UGH2, was used as a host. They found that the preferential alignment of $Ir(ppy)_2(acac)$ has a narrow orientation distribution of the molecular C_2 symmetry axis, with its maximum close to the normal direction, whereas $Ir(ppy)_3$ exhibits random orientation of its C_3 axis. Furthermore, they also estimate the degree of aggregation in $Ir(ppy)_2(acac)$-based guest–host systems, where the aggregates with an anti-parallel PDM alignment are formed above 10% dye content and they reduce SOP while keeping the TDM orientation unchanged.

Figure 5 plots the absolute value of the GSP slope versus the dipole moment p for films in previous studies.[10,18,39,40,56,57] The GSP slope is in the similar range of the electric field formed in the gases physisorbed on a cold surface (1–120 mV nm^{-1} at around 40 K), though the PDM intensity of organic semiconductors is typically greater than that of the gases.[26–29] In addition, unlike in the case of the physisorbed gases, most organic semiconductors exhibit positive GSP. The broken line in Fig. 5 indicates the average slope, excluding materials with extremely high slope ($Al(7\text{-}Prq)_3$, $Al(q\text{-}Cl)_3$) or low slope (DCJTB, $Ir(ppy)_3$, Znq_2, B3PyMPM, mCP). The slope, which corresponds to $\eta = n\langle \cos\theta \rangle / \varepsilon$, is considered in order to measure the efficiency of SOP formation per PDM. Interestingly, several materials, such as Alq_3, BCP, Bpy-OXD, and $Ir(ppy)_2(acac)$, plot close to the average slope, indicating that these materials form SOP with similar efficiencies. On the other hand, several materials, such as DCJTB, $Ir(ppy)_3$, Znq_2, B3PyMPM, and mCP, exhibit an extremely small η. Quantum chemical calculations revealed the electrostatic interaction energies (except dispersive forces) of a dimer of DCJTB, $Ir(ppy)_3$, Znq_2, and B3PyMPM are particularly strong, suggesting that these molecules are likely to form aggregates with vanishing PDM alignment.[39]

Although most materials show positive GSP (Fig. 5), negative GSP was also found in an evaporated film of an Alq_3 derivative. This negative GSP in $Al(7\text{-}Prq)_3$ film was discovered by Ref. 40. Since it is not only the molecular structure of $Al(7\text{-}Prq)_3$ that is similar to those of Alq_3,[18] but also PDM and molecular orbitals, it is surprising that a small change in the ligand sphere of the molecule, i.e., the attachment of propyl group, induces significant changes in GSP. This result suggests a possible mechanism for the formation of SOP. Reference 40 proposed an "asymmetric dice model", in which the statistics of stable positions of the molecule on the surface determine the molecular orientation.

The asymmetric dice model is consistent with the results recently reported by Ref. 41. They demonstrated that atomistic simulations mimic the GSP of several materials, and pointed out van der Waals interactions between the molecule and the surface during deposition to be the driving force of the anisotropic molecular orientation. Since the van der Waals force is valid within a short distance, the interactions are determined between the outermost parts of the molecule and those of adjacent molecules, where the shape of the molecule plays an important role.[64,65] They also reported that PDM interaction negatively contributes to

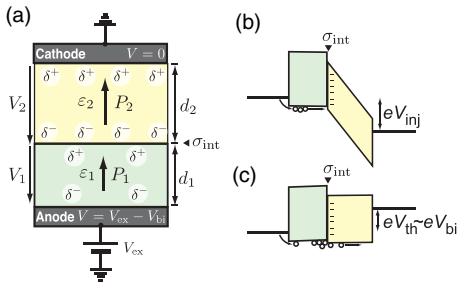

Figure 6. (Color online) (a) Schematic illustration of the orientation polarization in a bilayer device. The interface charge σ_{int} is induced at the organic heterointerface due to the orientation polarization. (b) Schematic illustrations of energy diagram at the hole injection voltage and (c) at the threshold voltage of the actual current. Adapted from Ref. 66.

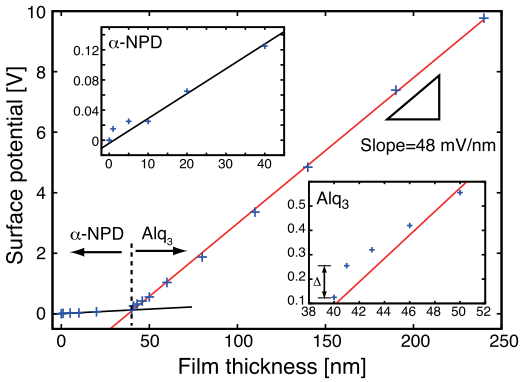

Figure 7. (Color online) The surface potential of the Alq_3 and α-NPD films as a function of film thickness. The Alq_3 film was deposited on an α-NPD film on an ITO substrate. The α-NPD/Alq_3 interface is located at a film thickness of 40 nm. The surface potential of the Alq_3 film grows linearly with a slope of 48 mV nm^{-1}, although a nonlinear region appears within several nanometers of the interface (bottom inset). The potential jump at the Alq_3/α-NPD interface (Δ) suggests the presence of an interface dipole. The α-NPD film also shows weak GSP behavior with a slope of ca. 5.3 mV nm^{-1} (top inset). Reprinted with permission from Ref. 16.

SOP formation, as suggested by several experimental results.[39,42,43]

3. Influences of SOP on the device properties

3.1. Interface charge model

The interface charge model describes how SOP affects the charge injection and accumulation behavior in the device.[11,12,16,20] We consider the charge injection voltage and charge accumulation characteristics of a bilayer device, where two organic layers with different polarization, $\mathbf{P}_1$ and $\mathbf{P}_2$, are sandwiched between the bottom and top electrodes [Fig. 6(a)]. For simplicity, only hole injection and accumulation are assumed in the following case.

The net polarization charge at the organic heterointerface is easily obtained as

$$\sigma_{int} = (\mathbf{P}_1 - \mathbf{P}_2) \cdot \hat{\mathbf{z}} = \varepsilon_1 \frac{V_{s1}}{d_1} - \varepsilon_2 \frac{V_{s2}}{d_2}, \tag{6}$$

where V_{s1}/d_1 and V_{s2}/d_2 correspond to the GSP slope of each film. Note that σ_{int} is independent of the film thicknesses. When the external voltage (V_{ex}) is applied to the bottom electrode with reference to the top electrode, $V_{ex} - V_{bi} = V_1 + V_2$ is valid, where V_1 and V_2 are the potential drop in the first and second layer, respectively, and V_{bi} is the built-in voltage. The built-in voltage originates from the work function difference between two electrodes and interface dipole at the contacts.[67] The electric field in the first layer should be positive when the hole injection from the bottom electrode occurs. This condition is independent from the energy barrier height at the electrode/organic film contact. The hole injection voltage (V_{inj}) is thus given by V_{ex} when $V_1/d_1 = 0$ [Fig. 6(b)], namely,

$$V_{inj} = V_{bi} + (\mathbf{P}_1 - \mathbf{P}_2) \cdot \hat{\mathbf{z}} \frac{d_2}{\varepsilon_2} = V_{bi} + \frac{\sigma_{int}}{\varepsilon_2} d_2, \tag{7}$$

where the boundary condition at the organic heterointerface,

$$\varepsilon_1 \frac{V_1}{d_1} + \mathbf{P}_1 \cdot \hat{\mathbf{z}} = \varepsilon_2 \frac{V_2}{d_2} + \mathbf{P}_2 \cdot \hat{\mathbf{z}}, \tag{8}$$

is used. Note that the hole injection voltage is proportional to the thickness of the second layer if σ_{int} is constant. This is the interface charge model proposed by Refs. 11, 12.

The injected holes into the first layer are accumulated at the organic heterointerface if the electric field in the second layer is negative. Note that this charge accumulation occurs regardless of the energy barrier height at the interface. When the conductance of the first layer is sufficiently high and the potential drop in the first layer is negligible small, the threshold voltage for hole injection into the second layer (V_{th}) equals V_{bi} [Fig. 6(c)]. The accumulated charge density at the interface at V_{th} is given by

$$\sigma_{acc} = (V_{th} - V_{inj}) \frac{\varepsilon_2}{d_2} = -\sigma_{int} \tag{9}$$

Therefore, the interface charge density can be estimated from the capacitance−voltage (C–V) measurement or displacement current measurement (DCM) of the bilayer device.[12,13] This simple model explains well the device characteristics below V_{th} and the correlation between the interface charge density and the GSP slope.[16]

3.2. Charge accumulation in bilayer devices

Figure 7 shows the surface potential characteristics of a bilayer structure of Alq_3 on the α-NPD layer as a function of film thickness.[16] The surface potential is measured with reference to the ITO substrate. Clear GSP behavior is observed with a slope of 48 mV nm^{-1} in the Alq_3 layer, and weak GSP behavior occurs with a slope of 5.3 mV nm^{-1} in the α-NPD layer. The net polarization charge induced at the interface is estimated to be -1.2 mC m^{-2} from Eq. (6). Here, the relative dielectric constants of 3.2 and 3.3 are used for the Alq_3 and α-NPD layers, respectively.

The estimated polarization charge density agrees well with the accumulation charge density at this interface. Figure 8 shows DCM curves of the α-NPD/Alq_3 bilayer device with various combinations of film thicknesses. DCM is a kind of C–V measurement in which a triangular wave voltage is applied to the device and current response including actual and displacement current is measured.[20,68–70] Since the displacement current is proportional to the apparent capacitance of the device, the charge injection and accumulation characteristics are examined. The accumulated charge density can be estimated by integrating the displacement current density from V_{acc} to V_{th}, i.e., 1.1 mC m^{-2}. This value is similar to the net polarization charge density (-1.2 mC m^{-2}) at this interface and is almost independent of the combination

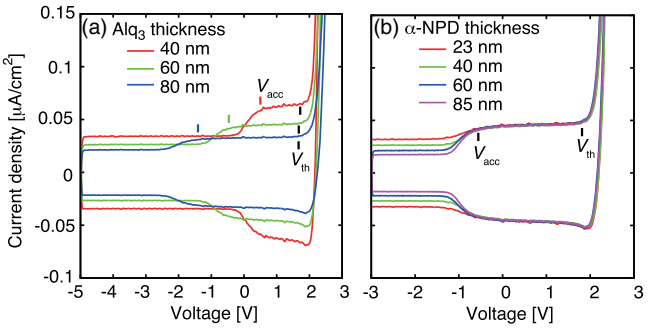

Figure 8. (Color online) (a), (b) DCM curves of the ITO/α-NPD/Alq_3/Al device for various film thicknesses. The α-NPD and Alq_3 film thicknesses are fixed at 40 nm (a) and 60 nm (b), respectively. The current density at the accumulation state depends only on the Alq_3 film thickness, indicating that the injected charges are holes. The threshold voltage of the actual current V_{th} is independent of the combinations of the film thickness, whereas V_{acc} shifts to the negative side with increasing Alq_3 film thickness. Thus, the polarity of interface charge is negative. Reprinted with permission from Ref. 16

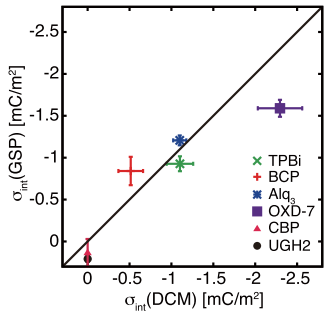

Figure 9. (Color online) Comparison between the interface charge density estimated from the GSP slope and DCM curves. The slope of the solid line is 1. Reproduced with permission from Ref. 16.

of the film thicknesses. Note that V_{acc} is considered to be the voltage at which the injected holes reach the interface, and from V_{inj} to V_{acc}, the injected holes accumulate in the bulk of the first layer, i.e., α-NPD, rather than the interface.[17,20] Therefore Eq. (9) is modified to determine the σ_{acc} from the DCM curves.

Similar results are obtained from the bilayer systems in which various polar molecules are used as the second layer. Figure 9 shows the relationship between the polarization charge density estimated from the GSP slope (σ_{int}(GSP)) and the interface charge density estimated from the DCM curves (σ_{int}(DCM)). The data points are located around the line with slope 1, indicating that the origin of the interface charge is the polarization charge due to SOP, and the polarization charge dominates the charge accumulation at the interface. Despite the limited number of materials that have been directly examined, if the device contains at least the materials shown in Fig. 2, the polarization charge should appear at the interface and modify charge accumulation properties.

OLEDs work at applied biases higher than V_{bi}. In this voltage region, the interface charge is compensated for by the injected counter charge. Thus the electric field due to the interface charge no longer affects device operation at least from the viewpoint of electrostatics. However, importantly, the interface charge is the polarization charge but the accumulated charge is the real charge. There are excess ionized molecules with the opposite polarity to the interface charge at the heterointerface. The ionized molecules near the emission zone can work as an exciton quencher and induce molecular decomposition.[48–52] On the other hand, the accumulated charge defines the emission zone and enhances the charge carrier balance factor.[44,71] Since the interface charge density is comparable to the maximum amount of the accumulation charge density during device operation,[44–47] this excess charge accumulation should be taken into account for detailed understanding of device operation and degradation mechanisms.

3.3. Charge injection at the metal/organic interface

The interface charge dominates the charge injection voltage and the minimum amount of accumulation charge density of a multilayer device during operation. Since the interface charge originates from SOP, there is a counter charge with the opposite polarity at the other interface of the film, e.g., the organic film/cathode interface in the case of the above-mentioned bilayer devices. The polarization charge at the interface can modify the interface properties, such as the energy level alignment and electronic structure,[54,72] and consequently the charge injection efficiency.[18,55]

Figure 10 shows the current-density–voltage–luminance (J–V–L) characteristics of Alq_3- and Al(7-Prq)$_3$-based devices. The device structure is ITO/α-NPD/Al(7-Prq)$_3$/Ca/Al and ITO/α-NPD/Alq_3/Ca/Al. Note that the polarity of SOP in the Al(7-Prq)$_3$ film is opposite that in the Alq_3 film (Figs. 2 and 5). The conductance of the Al(7-Prq)$_3$ device is remarkably low, which indicates the low charge carrier mobilities of the Al(7-Prq)$_3$ film and high resistance to the charge injection at the interfaces, i.e., α-NPD/Al(7-Prq)$_3$ for holes and Al(7-Prq)$_3$/Ca for electrons. The low charge carrier mobilities of the Al(7-Prq)$_3$ film are likely because an overlap of molecular orbitals between neighboring molecules may be hindered by the propyl group. Another possible reason for the poor bulk conductivity is the insufficient purity of the material, which can be a critical factor in charge transport characteristics. Moreover, high resistance to the electron injection at the Al(7-Prq)$_3$/Ca interface is suggested by the DCM curves.[18]

If we simply assume that the energy barrier for electron injection is the difference between the lowest unoccupied molecular orbital level and work function of Ca, no significant difference is observed between the Al(7-Prq)$_3$/Ca and Alq_3/Ca interfaces.[18] The origin of the high contact resistance can be attributed to the negative polarization charge at the Al(7-Prq)$_3$/Ca interface, which is the counterpart of the positive polarization charge at the α-NPD/Al(7-Prq)$_3$ interface [Figs. 10(b) and 10(c)]. The presence of the negative polarization charge can impede electron injection from the cathode to the Al(7-Prq)$_3$ layer. The device simulation based on the drift-diffusion model also revealed that the presence of the positive polarization charge at the cathode interface enhances electron injection.[55] Altazin et al. reported that the electron density is increased at the electron transport layer (ETL)/cathode interface, when the positive polarization charge is located at the interface. When the polarity is inverted, the electron density is decreased leading to a reduced conductivity of the ETL.

The influence of the polarity of SOP on the charge injection is further supported by the study of high-sensitivity ultraviolet photoemission spectroscopy. Reference 54 reported the direct observation of significantly relaxed negative

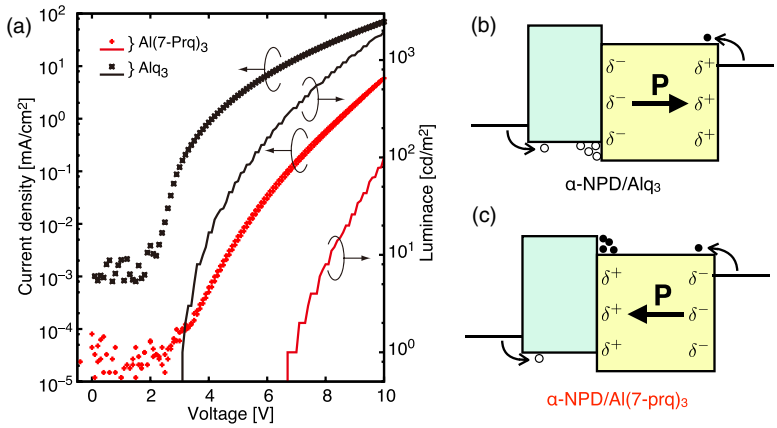

Figure 10. (Color online) (a) *J–V–L* characteristics of ITO/α-NPD/Al(7-Prq)$_3$/Ca/Al and ITO/α-NPD/Alq$_3$/Ca/Al devices. Adapted with permission from Ref. 18. (b), (c) Schematic energy diagram of the device in operation. The accumulated charge at the organic heterointerface is the hole in the Alq$_3$ device because of the negative polarization charge (b), whereas it is the electron in the Al(7-Prq)$_3$ device (c). At the ETL/cathode interface, the positive polarization charge exists for the Alq$_3$ device (b), which is negative for the Al(7-Prq)$_3$ device (c).

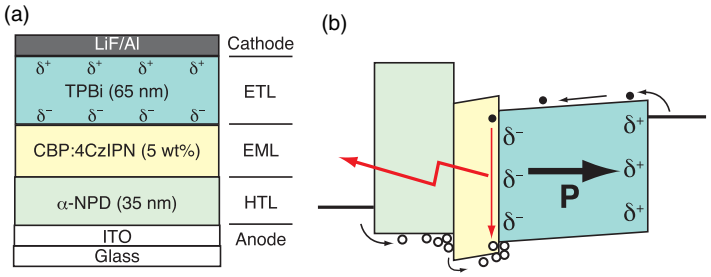

Figure 11. (Color online) (a) Schematic illustration of the device structure. (b) Schematic energy diagram of the device in operation.

carriers (anions) at the polar Alq$_3$ film surface. They showed that the electron detachment energy of the anion is about 1 eV larger than the electron affinity of Alq$_3$ measured by inverse photoemission. This significant relaxation energy leads to the good electron injection nature of Alq$_3$.

The polarity of SOP can play an important role in efficient charge injection, and a film with a positive orientation polarization, which corresponds to a positive polarization charge at the film surface, could be used as an electron injection layer (EIL). Interestingly, the polarity of SOP in ETL and EIL materials have always been found to be positive (Fig. 5), which is the preferable polarity for EIL, though they have been selected without knowledge of their relation with SOP.

3.4. SOP and device degradation

The apparent interface charge density works as a sensitive probe for device degradation; it decreases proportionally to the loss of luminous efficiency. This relation was first found by Ref. 73 in an Alq$_3$-based OLED, and following studies revealed similar behavior in other device structures incorporating SOP films.[17,19,48,74,75] Because the interface charge adjacent to the emission layer (EML) confines the emission zone of the device due to the charge accumulation nature,[19] it seems reasonable that the apparent interface charge density is sensitive to the changes (generation of charge traps, change of orientation polarization and so on) in the emission zone. In this section, we show some examples of the degradation properties of OLEDs which include SOP film as an ETL.

The first example is the device doped with a TADF emitter, 4CzIPN.[36] The device structure is ITO/α-NPD/CBP:4CzIPN (5wt%)/TPBi/LiF/Al [Fig. 11(a)]. Because of SOP of the TPBi layer, hole accumulation occurs at the EML/ETL interface at the voltages lower than the electron injection voltage that is around V_{th}. Thus the recombination zone is expected to be confined at the EML/ETL interface [Fig. 11(b)]. Because α-NPD strongly quenches the triplet exciton of 4CzIPN through the Dexter energy transfer,[53] keeping the recombination zone far from α-NPD leads to improved EL efficiency.

Figure 12(a) shows the aging curves of this device at constant aging current of 12.5 mA cm^{-2}. Luminance is normalized by the initial luminance. The normalized luminance decays rapidly although the driving voltage increases slightly, indicating that the hole transport layer and ETL did not degrade significantly. Figure 12(b) shows the DCM curves measured at different aging times. V_{inj} shifts to higher voltages with device aging, whereas V_{th} stays at the initial voltage, indicating that σ_{acc} decreased. In Fig. 12(c), we plotted the normalized luminance and normalized σ_{acc} and observed an excellent linear relation with slope equal to 1. The result strongly suggests that the charge accumulation is closely related to the luminance loss in the device. Similar linear relations have been reported in devices with polar films such as Alq$_3$.[17,73–75] Charge accumulation often correlates with degradation phenomena in various OLEDs.[48,51] It appears that σ_{acc} evaluation is useful for measuring device degradation.

The reduction in σ_{acc} may be caused by the trapped holes near the EML/ETL interface and disordering of molecular orientation in ETL. Charge traps are often generated during

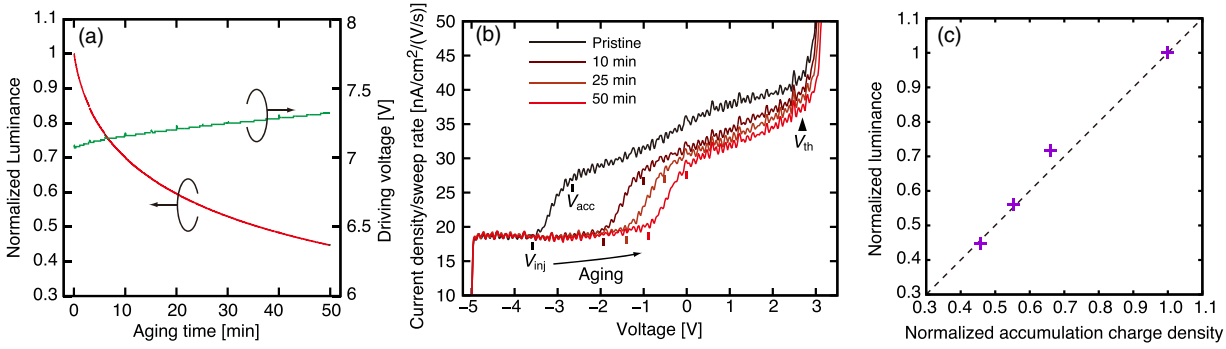

Figure 12. (Color online) (a) Aging curves of the doped device at a constant current of 12.5 mA cm^{-2}. Luminance is normalized by the initial luminance (left axis). The driving voltage is also shown (right axis). (b) Typical DCM curves in the forward sweep of the doped devices at various aging times (10 V/s). (c) Relation between the normalized luminance and normalized accumulation charge density. The accumulation charge density was estimated by integrating the DCM curve from V_{acc} to V_{inj} and normalized by the value of the pristine device. The broken line has a slope of 1. Reprinted with permission from Ref. 18.

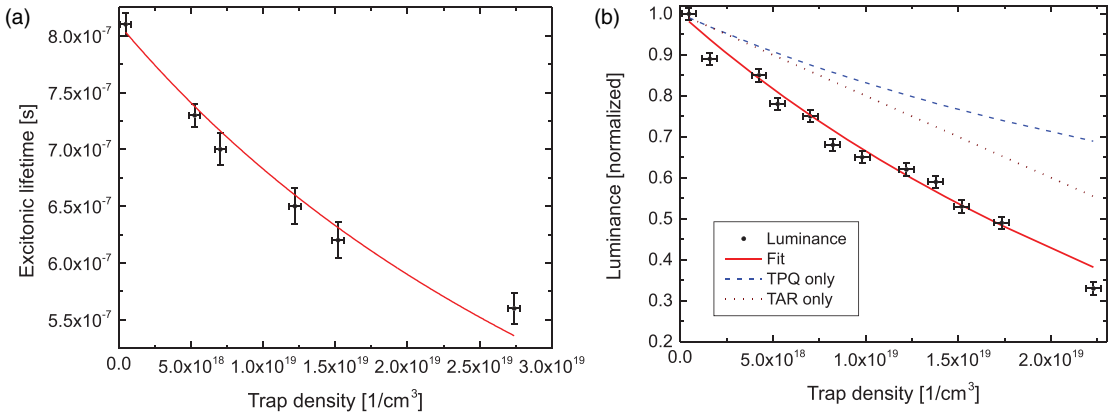

Figure 13. (Color online) (a) Crosses: lifteimes of excited states from the TRELS experiments as a function of the trapped charge density determined via DCM investigations. Solid line: Fit of the experimental data using the modified TPQ model. The fit describes the measured data in an excellent way and results in a reasonable value for a TPQ rate of $(0.23 \pm 0.03) \times 10^{-13}$ cm^3 s^{-1}. (b) Normalized luminance as a function of trapped charge density (crosses). The red line represents the fit including the individual contributions of TPQ (blue dashed line) and TAR (brown dotted line), respectively. Adapted with permission from Ref. 75.

device degradation, e.g., due to decomposition and the chemical reactions of molecules.[48,51)] The holes captured at such traps compensate for the negative polarization charge due to the SOP of TPBi; as the result, the apparent interface charge density decays.[18,73)] On the other hand, the molecular orientation, consequently SOP, can also be changed, possibly by the high temperature during device operation due to Joule's heating and non-radiative recombination.[76)] Both cases have been reported; however, the efficiency loss can be attributed to the generation of charge traps.

Reference 75 reported a correlation of the trapped charge density and emission loss in a phosphorescent OLED (Fig. 13). The device structure they studied was ITO/HATCN/α-NPD/Ir(ppy)$_3$:CBP (6.5wt%)/BPhen/Ca/Al, where BPhen exhibits SOP like BCP. They conducted a combination study of time-resolved electroluminescence spectroscopy (TRELS) and DCM. The DCM characteristics of this device are essentially similar to those of the TADF-OLED (Fig. 12); i.e., the charge accumulation occurs at the EML/ETL interface and σ_{acc} proportionally decreased with the luminous efficiency. Although the reduction of σ_{acc} does not directly indicate the presence of the trapped holes as mentioned previously, DCM can also evaluate the trapped charge density by considering the shift in the DCM curves of the first and subsequent triangular voltage sweeps.[19,20)] The estimated trapped hole density also has a linear relation with luminous efficiency. The exciton lifetime decay evaluated by TRELS is explained well by considering the non-radiative recombination due to the traps via the triplet-polaron quenching (TPQ) process [Fig. 13(a)].[52)] However, the presence of TPQ does not fully explain the total luminance loss observed in this device; thus additional mechanisms of efficiency loss such as trap-assisted recombination (TAR),[77)] which deteriorates the carrier balance factor, should also be considered [Fig. 13(b)].

Many electron transporting and emitting materials exhibit SOP.[39)] In the guest–host system, SOP is even enhanced depending on the mixing ratio.[42,43)] In order to properly control charge distribution around the emission zone, it is necessary to understand the SOP characteristics of ETL and EML. The charge concentration at the EML interface confines the recombination zone, leading to fast degradation.[53)] Therefore, a broad interface, which is formed by intermixing the EML with ETL, can improve device stability,[78–80)] as it dilutes the polarization charge density, and consequently the exciton concentration. Controlling the polarization charge distribution and the energy offset by the appropriate choice of the materials and interface design is important for ensuring stable operation of OLEDs.

4. Conclusions

We have reviewed the current understanding of SOP in the evaporated films of polar organic semiconductors and its influence on the properties of OLEDs. SOP is inherent in the evaporated film of many common OLED materials, mainly electron transporters and various kinds of emitters. The results can be extended to many other polar molecules of organic semiconductors. The mechanism of SOP formation is, however, still not completely understood. Currently, the short-range van der Waals interaction at the surface during molecular deposition has been suggested to be the driving force of the anisotropic molecular orientation, while the PDM interaction is considered to be a negative factor.

Because of the polarization charge induced at heterointerfaces, SOP modifies the interface properties such as charge accumulation and injection of the device. The interface charge density defines the minimum amount of the accumulated charge during device operation, and that is comparable to the maximum amount of the total charge density. Importantly, the accumulated charge is the real charge while the interface charge is the polarization charge. The emission zone is confined near the charge accumulation interface but the presence of the excess charged species near the emission zone often acts as an exciton quencher and induces decomposition of the molecules. Besides the energy level offset and the difference of charge carrier mobilities at the organic heterointerfaces, the charge accumulation properties of the device should be managed, taking into account the SOP of each layer. On the other hand, the counterpart of the interface charge is located at the organic film/cathode interface if the polar film is used as the electron injection layer. The presence of positive polarization charge can enhance the electron injection efficiency. The use of positive GSP materials such as EIL is therefore a reasonable choice in terms of the polarity of the film. Although SOP has not been considered as a significant factor in device performance, in terms of device optimization, the orientational order of PDMs in the film should be taken into account as an intrinsic material property.

It is worth mentioning that SOP is significantly quenched in neat films. There is considerable potential for enhancement of the orientation polarization, though the mechanism of GSP build-up needs to be clarified. Controlling SOP based on the molecular design would be an important achievement for the improvement of device performance and for exploiting innovative functions of organic semiconductors.

We note here additional information found during the review process of this paper. The GSP slope of three additional materials were measured: 3TPYMB (2.87 D, 48 mV nm^{-1}), 6FAlq$_3$ (5.46 D, 29 mV nm^{-1}), and FIrpic (7.72 D, 14 mV nm^{-1}). A negative GSP slope of -32 mV nm^{-1} was also observed for BAlq$_3$. The polarity is opposite of that in the previous study.[39] The origin of polarization flipping is currently under investigation. Two papers regarding SOP were published very recently.[81,82] One reports on the origin of anisotropic molecular packing in vapor-deposited Alq$_3$ glasses.[81] The other shows the enhancement of electron injection due to the polarization charge.[82]

Acknowledgments

The authors gratefully acknowledge the students and researchers who contributed to the works reviewed in this paper. This research is partly supported by the Japan Society for the Promotion of Science (JSPS) KAKENHI (Grant Nos. 15K13293 and 16H04222), and the Institute of Science and Technology Meiji University, Designated Research, Japan. This work was also supported by a grant from the Deutsche Forschungsgemeinschaft (DFG; contract no. BR1728/20-1). Furthermore, WB acknowledges JSPS for a BRIDGE Fellowship. The quantum chemical calculations were partly performed at the Research Center for Computational Science, Okazaki, Japan.

Appendix

Material abbreviations

- **Alq$_3$**: tris-(8-hydroxyquinolate) aluminum
- **Al(q-Cl)$_3$**: tris(5-chloro-8-hydroxyquinolinato) aluminum
- **Al(7-Prq)$_3$**: tris(7-propyl-8-hydroxyquinolinolato) aluminum(III)
- **BAlq**: bis(2-methyl-8-quinolinolate)-4-(phenylphenolato)aluminum
- **BCP**: 2,9-dimethyl-4,7-diphenyl-1,10-phenanthroline
- **BPhen**: 4,7-Diphenyl-1,10-phenanthroline
- **Bpy-OXD**: 1,3-bis[2-(2,2′-bipyridine-6-yl)-1,3,4-oxadiazo-5-yl]benzene
- **B3PyMPM**: bis-4,6-(3,5- di-3-pyridylphenyl)-2-methylpyrimidine
- **CBP**: 4,4′-bis(N-carbazolyl)-1,1′-biphenyl
- **DACT-II**: 9-[4-(4,6-diphenyl-1,3,5-triazin-2-yl)phenyl]-N,N,N′,N′-tetraphenyl-9H-carbazole-3,6-diamine
- **DCJTB**: 4-[dicyanomethylene]-2-tert-butyl-6-(1,1,7,7-tetramethyljulolidyl-9-enyl)-4H-pyran
- **FIrpic**: bis(3,5-difluoro-2-(2-pyridyl)phenyl-(2-carboxypyridyl)iridium(III)
- **Gaq$_3$**: tris(8-hydroxyquinolinato) gallium(III)
- **HATCN**: Hexa-azatriphenylene-hexanitrile
- **Ir(ppy)$_2$(acac)**: bis[2-(2-pyridinyl-N)phenyl-C](acetylacetonate) iridium(III)
- **Ir(ppy)$_3$**: tris(2-phenylpyridine) iridium(III)
- **ITO**: indium-tin-oxide
- **mCP**: 1,3-Bis(N-carbazolyl)benzene
- **OXD-7**: 1,3-bis[2-(4-tert-butylphenyl)-1,3,4-oxadiazo-5-yl]benzene
- **TPBi**: 1,3,5-tris(1-phenyl-1H-benzimidazol-2-yl)benzene
- **UGH2**: 1,4-bis-(triphenylsilyl)benzene
- **Znq$_2$**: bis(8-hydroxyquinoline) zinc
- **2CzPN**: 1,2-bis(carbazol-9-yl)-4,5-dicyanobenzene
- **3TPYMB**: tris(2,4,6-trimethyl-3-(pyridin-3-yl)phenyl) borane
- **4CzIPN**: 1,2,3,5-Tetrakis(carbazol-9-yl)-4,6-dicyanobenzene
- **4CzPN**: 1,2,3,4-tetrakis(carbazol-9-yl)-5,6-dicyanobenzene
- **6FAlq$_3$**: tris(6-fluoro-8-hydroxy-quinolinato)aluminumα
- **α-NPD**: N,N′-bis(1-naphthyl)-N,N′-diphenyl-1,1′-biphenyl-4,4′-diamine (This molecule is commonly

referred to as "α-NPD", though its molecular structure is identical to "NPB").

1) "Various spectroscopic studies on molecular orientation were reported by using vibrational spectroscopy, X-ray absorption spectroscopy, etc. For example, K. Seki, H. Ishii, and Y. Ouchi, in *Chemical Applications of Synchrotron Radiation*, ed. T.-K. Sham, (World Scientific, Singapore, 2002), Chap. 8.
2) D. Yokoyama, A. Sakaguchi, M. Suzuki, and C. Adachi, Org. Electron. **10**, 127 (2009).
3) D. Yokoyama, J. Mater. Chem. **21**, 19187 (2011).
4) D. Yokoyama, A. Sakaguchi, M. Suzuki, and C. Adachi, Appl. Phys. Lett. **95**, 243303 (2009).
5) J. Frischeisen, D. Yokoyama, C. Adachi, and W. Brütting, Appl. Phys. Lett. **96**, 073302 (2010).
6) D. Yokoyama, H. Sasabe, Y. Furukawa, C. Adachi, and J. Kido, Adv. Funct. Mater. **21**, 1375 (2011).
7) J. Frischeisen, D. Yokoyama, A. Endo, C. Adachi, and W. Brütting, Org. Electron. **12**, 809 (2011).
8) W. Brütting, J. Frischeisen, T. D. Schmidt, B. J. Scholz, and C. Mayr, Phys. Status Solidi A **210**, 44 (2013).
9) T. D. Schmidt, T. Lampe, M. R. Daniel Sylvinson, P. I. Djurovich, M. E. Thompson, and W. Brütting, Phys. Rev. Appl. **8**, 037001 (2017).
10) E. Ito, Y. Washizu, N. Hayashi, H. Ishii, N. Matsuie, K. Tsuboi, Y. Ouchi, Y. Harima, K. Yamashita, and K. Seki, J. Appl. Phys. **92**, 7306 (2002).
11) S. Berleb, W. Brütting, and G. Paasch, Org. Electron. **1**, 41 (2000).
12) W. Brütting, S. Berleb, and A. G. Mückl, Org. Electron. **2**, 1 (2001).
13) Y. Noguchi, N. Sato, Y. Tanaka, Y. Nakayama, and H. Ishii, Appl. Phys. Lett. **92**, 203306 (2008).
14) Y. Noguchi, N. Sato, Y. Miyazaki, and H. Ishii, Appl. Phys. Lett. **96**, 143305 (2010).
15) Y. Noguchi, N. Sato, Y. Miyazaki, Y. Nakayama, and H. Ishii, Jpn. J. Appl. Phys. **49**, 01AA01 (2010).
16) Y. Noguchi, Y. Miyazaki, Y. Tanaka, N. Sato, Y. Nakayama, T. D. Schmidt, W. Brütting, and H. Ishii, J. Appl. Phys. **111**, 114508 (2012).
17) Y. Noguchi, T. Tamura, H.-J. Kim, and H. Ishii, J. Photonics Energy **2**, 021214 (2012).
18) Y. Noguchi et al., Appl. Phys. Lett. **102**, 203306 (2013).
19) Y. Noguchi, H.-J. Kim, R. Ishino, K. Goushi, C. Adachi, Y. Nakayama, and H. Ishii, Org. Electron. **17**, 184 (2015).
20) Y. Noguchi, Y. Tanaka, Y. Miyazaki, N. Sato, Y. Nakayama, and H. Ishii, in *Physics of Organic Semiconductors*, ed. W. Brütting and C. Adachi (Weinheim, Wiley, 2012), Chap. 5.
21) K. Kutzner, Thin Solid Films **14**, 49 (1972).
22) L. Onsager, D. Staebler, and S. Mascarenhas, J. Chem. Phys. **68**, 3823 (1978).
23) J. Chrzanowski and B. Sujak, Thin Solid Films **79**, 101 (1981).
24) M. J. Iedema, M. J. Dresser, D. L. Doering, J. B. Rowland, W. P. Hess, A. A. Tsekouras, and J. P. Cowin, J. Phys. Chem. B **102**, 9203 (1998).
25) R. Balog, P. Cicman, N. C. Jones, and D. Field, Phys. Rev. Lett. **102**, 073003 (2009).
26) O. Plekan, A. Cassidy, R. Balog, N. C. Jones, and D. Field, Phys. Chem. Chem. Phys. **13**, 21035 (2011).
27) A. Cassidy, O. Plekan, R. Balog, N. C. Jones, and D. Field, Phys. Chem. Chem. Phys. **15**, 108 (2013).
28) A. Cassidy, O. Plekan, R. Balog, J. Dunger, D. Field, and N. C. Jones, J. Phys. Chem. A **118**, 6615 (2014).
29) C. Bu, J. Shi, U. Raut, E. H. Mitchell, and R. A. Baragiola, J. Chem. Phys. **142**, 134702 (2015).
30) I. K. Gavra, A. N. Pilidi, and A. A. Tsekouras, J. Chem. Phys. **146**, 104701 (2017).
31) T. Manaka, K. Yoshizaki, and M. Iwamoto, Curr. Appl. Phys. **6**, 877 (2006).
32) K. Yoshizaki, T. Manaka, and M. Iwamoto, J. Appl. Phys. **97**, 023703 (2004).
33) K. Ozasa, H. Ito, M. Maeda, and M. Hara, Appl. Phys. Lett. **98**, 013301 (2011).
34) K. Sugi, H. Ishii, Y. Kimura, M. Niwano, E. Ito, Y. Washizu, N. Hayashi, Y. Ouchi, and K. Seki, Thin Solid Films **464–465**, 412 (2004).
35) N. Kajimoto, T. Manaka, and M. Iwamoto, Chem. Phys. Lett. **430**, 340 (2006).
36) H. Uoyama, K. Goushi, K. Shizu, H. Nomura, and C. Adachi, Nature **492**, 234 (2012).
37) C. Adachi, Jpn. J. Appl. Phys. **53**, 060101 (2014).
38) H. Kaji et al., Nat. Commun. **6**, 8476 (2015).
39) K. Osada, K. Goushi, H. Kaji, C. Adachi, H. Ishii, and Y. Noguchi, Org. Electron. **58**, 313 (2018).
40) T. Isoshima, Y. Okabayashi, E. Ito, M. Hara, W. W. Chin, and J. W. Han, Org. Electron. **14**, 1988 (2013).
41) P. Friederich, V. Rodin, F. Von Wrochem, and W. Wenzel, ACS Appl. Mater. Interfaces **10**, 1881 (2018).
42) L. Jäger, T. D. Schmidt, and W. Brütting, AIP. Adv. **6**, 095220 (2016).
43) T. Morgenstern, M. Schmid, A. Hofmann, M. Bierling, L. Jäger, and W. Brütting, ACS Appl. Mater. Interfaces **10**, 31541 (2018).
44) B. Ruhstaller, S. A. Carter, S. Barth, H. Riel, W. Riess, and J. C. Scott, J. Appl. Phys. **89**, 4575 (2001).
45) M. Matsumura, A. Ito, and Y. Miyamae, Appl. Phys. Lett. **75**, 1042 (1999).
46) F. Rohlfing, T. Yamada, and T. Tsutsui, J. Appl. Phys. **86**, 4978 (1999).
47) D. Taguchi, S. Inoue, L. Zhang, J. Li, M. Weis, T. Manaka, and M. Iwamoto, J. Phys. Chem. Lett. **1**, 803 (2010).
48) S. Scholz, D. Kondakov, B. Lüssem, and K. Leo, Chem. Rev. **115**, 8449 (2015).
49) R. H. Young, C. W. Tang, and A. P. Marchetti, Appl. Phys. Lett. **80**, 874 (2002).
50) D. Y. Kondakov, W. C. Lenhart, and W. F. Nichols, J. Appl. Phys. **101**, 024512 (2007).
51) F. So and D. Kondakov, Adv. Mater. **22**, 3762 (2010).
52) C. Murawski, K. Leo, and M. C. Gather, Adv. Mater. **25**, 6801 (2013).
53) H. Nakanotani, K. Masui, J. Nishide, T. Shibata, and C. Adachi, Sci. Rep. **3**, 2127 (2013).
54) H. Kinjo, H. Lim, T. Sato, Y. Noguchi, Y. Nakayama, and H. Ishii, Appl. Phys. Exp. **9**, 021601 (2016).
55) S. Altazin, S. Züfle, E. Knapp, C. Kirsch, T. D. Schmidt, L. Jäger, Y. Noguchi, W. Brütting, and B. Ruhstaller, Org. Electron. **39**, 244 (2016).
56) N. Hayashi, K. Imai, T. Suzuki, K. Kanai, Y. Ouchi, and K. Seki, IPAP Conf. Series **6**, 69 (2004).
57) M. Kröger, S. Hamwi, J. Meyer, T. Dobbertin, T. Riedl, W. Kowalsky, and H. H. Johannes, Phys. Rev. B **75**, 235321 (2007).
58) D. Yokoyama, K.-I. Nakayama, T. Otani, and J. Kido, Adv. Mater. **24**, 6368 (2012).
59) J. W. Sun, J. H. Lee, C. K. Moon, K. H. Kim, H. Shin, and J. J. Kim, Adv. Mater. **26**, 5684 (2014).
60) S. Y. Kim, W. I. Jeong, C. Mayr, Y. S. Park, K. H. Kim, J. H. Lee, C. K. Moon, W. Brütting, and J. J. Kim, Adv. Funct. Mater. **23**, 3896 (2013).
61) K. H. Kim, C. K. Moon, J. W. Sun, B. Sim, and J. J. Kim, Adv. Opt. Mater. **3**, 895 (2015).
62) J. W. Sun, K. H. Kim, C. K. Moon, J. H. Lee, and J. J. Kim, ACS Appl. Mater. Interfaces **8**, 9806 (2016).
63) C. Murawski, C. Elschner, S. Lenk, S. Reineke, and M. C. Gather, Org. Electron. **53**, 198 (2018).
64) M. J. Jurow, C. Mayr, T. D. Schmidt, T. Lampe, P. I. Djurovich, W. Brütting, and M. E. Thompson, Nat. Mater. **15**, 85 (2016).
65) C. K. Moon, K. H. Kim, and J. J. Kim, Nat. Commun. **8**, 791 (2017).
66) Y. Noguchi, Y. Nakayama, and H. Ishii, J. Vac. Soc. Jpn. **58**, 37 (2015).
67) H. Ishii, K. Sugiyama, E. Ito, and K. Seki, Adv. Mater. **11**, 605 (1999).
68) S. Egusa, A. Miura, N. Gemma, and M. Azuma, Jpn. J. Appl. Phys. **33**, 2741 (1994).
69) S. Ogawa, Y. Kimura, H. Ishii, and M. Niwano, Jpn. J. Appl. Phys. **42**, L1275 (2003).
70) Y. Noguchi, T. Higeta, and F. Yonekawa, Adv. Opt. Mater. **6**, 1800318 (2018).
71) G. G. Malliaras and J. C. Scott, J. Appl. Phys. **85**, 7426 (1999).
72) Y. Nakayama, S. Machida, Y. Miyazaki, T. Nishi, Y. Noguchi, and H. Ishii, Org. Electron. **13**, 2850 (2012).
73) D. Y. Kondakov, J. R. Sandifer, C. W. Tang, and R. H. Young, J. Appl. Phys. **93**, 1108 (2003).
74) V. V. Jarikov and D. Y. Kondakov, J. Appl. Phys. **105**, 034905 (2009).
75) T. D. Schmidt, L. Jäger, Y. Noguchi, H. Ishii, and W. Brütting, J. Appl. Phys. **117**, 215502 (2015).
76) T. Miyamae, N. Takada, T. Yoshioka, S. Miyaguchi, H. Ohata, and T. Tsutsui, Chem. Phys. Lett. **616–617**, 86 (2014).
77) M. Kuik, L. J. A. Koster, G. A. H. Wetzelaer, and P. W. M. Blom, Phys. Rev. Lett. **107**, 256805 (2011).
78) Z. D. Popovic, H. Aziz, C. P. Tripp, N.-X. Hu, A.-M. Hor, and G. Xu, Proc. SPIE **3476**, 3476 (1998).
79) J. H. Lee, S. W. Liu, C.-A. Huang, K. H. Yang, and Y. Chang, Proc. SPIE **5464**, 5464 (2004).
80) M. Minagawa and N. Takahashi, Jpn. J. Appl. Phys. **55**, 02BB08 (2016).
81) K. Bagchi, N. E. Jackson, A. Gujral, C. Huang, M. F. Toney, L. Yu, J. J. D. Pablo, and M. D. Ediger, J. Phys. Chem. Lett. **10**, 164 (2019).
82) Y. Tanaka, T. Makino, and H. Ishii, Trans. Electron. **E102-C**, 172 (2019).

